

Electrical Stability and Performance of a Nitrogen–Oxygen Atmospheric Pressure Gliding Arc Plasma

Filippo Manaigo,* Omid Samadi Bahnamiri, Abhyuday Chatterjee, Adriano Panepinto, Arnaud Krumpmann, Matthieu Michiels, Annemie Bogaerts, and Rony Snyders



Cite This: *ACS Sustainable Chem. Eng.* 2024, 12, 5211–5219



Read Online

ACCESS |



Metrics & More



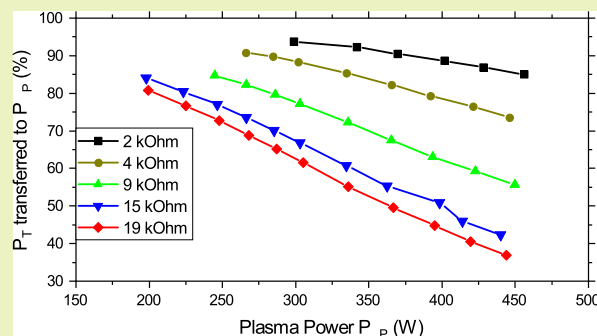
Article Recommendations



Supporting Information

ABSTRACT: Nonthermal plasmas are currently being studied as a green alternative to the Haber–Bosch process, which is, today, the dominant industrial process allowing for the fixation of nitrogen and, as such, a fundamental component for the production of nitrogen-based industrial fertilizers. In this context, the gliding arc plasma (GAP) is considered a promising choice among nonthermal plasma options. However, its stability is still a key parameter to ensure industrial transfer of the technology. Nowadays, the conventional approach to stabilize this plasma process is to use external resistors. Although this indeed allows for an enhancement of the plasma stability, very little is reported about how it impacts the process efficiency, both in terms of NO_x yield and energy cost. In this work, this question is specifically addressed by studying a DC-powered GAP utilized for nitrogen fixation into NO_x at atmospheric pressure stabilized by variable external resistors. Both the performance and the stability of the plasma are reported as a function of the utilization of the resistors. The results confirm that while the use of a resistor indeed allows for a strong stabilization of the plasma without impacting the NO_x yield, especially at high plasma current, it dramatically impacts the energy cost of the process, which increases from 2.82 to 7.9 MJ/mol. As an alternative approach, we demonstrate that the replacement of the resistor by an inductor is promising since it allows for decent stabilization of the plasma, while it does not affect either the energy cost of the process or the NO_x yield.

KEYWORDS: IR, NMR, UV, plasma-based nitrogen fixation, energy cost, arc stabilization, external passive components, power dissipation

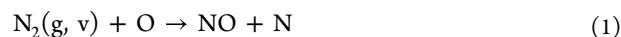


INTRODUCTION

Nitrogen is an essential element for any living organism: as an example, daily, an average person consumes almost 11 g of nitrogen.¹ In nature, nitrogen is mostly found in its molecular form as N₂, which makes up 78% of the atmosphere. However, due to the high energy needed to break its strong triple bond (9.756 eV bond dissociation energy²), it cannot be directly accessible to most living organisms and must be converted into more reactive N-containing compounds, such as nitric oxide (NO), nitrogen dioxide (NO₂), ammonia (NH₃), etc. in a process known as “nitrogen fixation”. For this reason, nitrogen fixation is also a mandatory step in the synthesis of N-based artificial fertilizers.³ Today, the demand for industrially fixated nitrogen is mostly addressed by the Haber–Bosch (H–B) process, which allows for the catalytic synthesis of NH₃ at high temperatures (650–750 K) and high pressures of around 100 bar.⁴ In addition, in order to make the process economically viable, large centralized H–B facilities are necessary.⁵ Given the large scale in which it is globally used and despite its good energy efficiency, the H–B process currently consumes approximately 1% of the world energy production and emits around 300 million tons of carbon dioxide (CO₂) each year,⁶ which corresponds to approximately 1% of the CO₂ emissions

in 2019.⁷ It is therefore necessary to develop alternative nitrogen fixation processes that would allow for a lower energy consumption and a reduced environmental impact.

In this context, plasma-based nitrogen fixation approaches are gaining a lot of interest as a complementary method for the production of reactive nitrogen-based molecules, thanks to the possibility of selectively channeling energy to the most efficient pathway, allowing for an energy cost-effective production of nitrogen compounds, especially nitrogen oxides (NO_x).⁸ The chemistry leading to NO_x formation in nonthermal plasmas is well-known and widely described.^{4,8,9} The main net contributor to the NO_x formation is the Zeldovich mechanism, which consists of breaking of the triple bond of N₂, either in the ground state or vibrationally excited with an O atom.

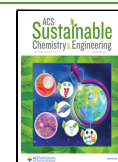


Received: December 15, 2023

Revised: March 2, 2024

Accepted: March 4, 2024

Published: March 16, 2024



where g stands for the ground state and v indicates a vibrationally excited state.

It should be noted that the Zeldovich reaction can occur from both $N_2(g)$ and $N_2(v)$. In the first case, it is defined as the thermal Zeldovich mechanism, while in the second case, it is called the “vibrationally enhanced Zeldovich mechanism”.⁹ In warm plasmas, such as the GAP, the thermal Zeldovich mechanism is expected to be dominant because of the high gas temperature of several 1000 K.

The N atom is further involved in a reaction with O_2 in either ground state or vibrationally excited



NO_2 is then mainly formed in either the discharge region as the NO reacts with the O atoms



or, as the gas cools down, in the postdischarge region through NO oxidation



Considering this formation mechanism, the theoretical limit for the energy consumption for N_2 oxidative fixation with nonthermal plasmas is stated to be lower than the current energy consumption reached with the H–B process (0.48 MJ/mol) and the theoretical limit of the H–B process (0.35 MJ/mol).⁴ It should be realized that we can in fact not directly compare the process of plasma-based NO_x production to the H–B process; NH_3 synthesis from N_2 and H_2 . Indeed, although NH_3 and NO_x are both molecules relevant for nitrogen fixation, they are very different. The energy cost of NH_3 production is intrinsically high because the energy content is much higher. Indeed, NH_3 production through H–B makes necessary the use of H_2 which is currently still mainly produced through steam reforming of methane consuming a huge quantity of energy and generating strong CO_2 emissions. Furthermore, the H–B process also requires energy because of the reaction conditions (high temperature to overcome the energy barrier), although this is only a fraction of what is needed for H_2 production, and the energy requirement is further reduced thanks to heat integration. Subsequently, NO_x is produced in the classical process via the oxidation of NH_3 in the highly exothermic Ostwald process ($NH_3 + O_2 \rightarrow NO_x + H_2O$). In contrast, plasma-based NO_x production directly from air ($N_2 + O_2 \rightarrow NO_x$) is endergonic. This is made possible by the plasma power, while in the classical process, it is possible by using NH_3 instead of N_2 , hence by making use of the downhill (exothermic and exergonic) oxidation of the H atoms. Therefore, it is not easy to directly compare plasma-based NO_x production with the classical process (three steps) in terms of thermodynamics. That is why in plasma-based NO_x production literature, the energy cost is always defined in terms of moles of fixated nitrogen. An additional advantage is that the plasma-based process facilities would be easier to implement compared to the ones required for the H–B process, allowing for the implementation of smaller-scale local fertilizer production facilities compatible with the usage of renewable energy sources allowing for a strong reduction of the distribution costs.¹⁰ In this context, encouraging results have been achieved with microwave (MW) plasmas where a yield of 7% of NO was obtained at reduced pressures between 0.5 to 15 Torr. The energy cost (EC) was, however, estimated to be around 8 MJ/mol without taking into account the energy

dissipated in the pumping system.¹¹ Recently, very good results were also obtained in a MW plasma at atmospheric pressure, at relatively high power (1 kW) and flow rates (up to 20 slm), yielding 3.8% NO_x , an EC as low as 2.0 MJ/mol, and quite high NO_x production rates of 0.77 slm.¹² From an energy efficiency perspective, the current best result of 0.42 MJ/mol has been obtained with a pulsed plasma jet,¹³ which, despite the relatively low yield of 0.02%, shows a lower energy consumption than the H–B process. Catalysts have also been used to further improve the performance of plasma processes. As an example, a DC glow discharge, operated with an Al_2O_3 powder of about 75 μm diameter, showed a total NO_x yield of 0.7% and an EC of 2.8 MJ/mol.¹⁴

Gliding arc plasmatrons (GAPs) are among the most promising plasma reactor types for gas conversion. The reason is that they operate at atmospheric pressure, making them easy to implement on an industrial scale and provide reduced electric fields below 100 Td, which is beneficial for the production of fixated nitrogen as it favors the vibrational excitation over more energetic processes such as electronic excitation or ionization.^{15,16} Recent studies focusing on the understanding of the fundamental plasma chemistry in a GAP have been published, and a thoughtful explanation of the arc dynamics¹⁷ and the flux behavior in between the electrodes¹⁸ offers valuable insight into the importance of increasing the gas fraction interacting with the arc for more efficient gas conversion. Concerning its application for nitrogen fixation, a maximum NO_x yield of 1.5% at an EC of 3.6 MJ/mol was obtained with a GAP.⁹ However, the best results so far have been obtained with a rotating gliding arc (RGA), a slightly different configuration of the GAP discussed in this work, showing a NO_x yield of 5.5% and a corresponding EC of 2.5 MJ/mol without the presence of any catalysts.¹⁶ The performance can be further improved by favoring NO_2 formation (eq 3) over the Zeldovich back-reaction that would cause the dissociation of the produced NO, which at atmospheric pressure is dominant with a gas temperature above approximately 2700 K.¹⁹ This was done (i) by adding an effusion nozzle, which enhanced the cooling of the gas temperature, improving the RGA performance to a NO_x yield of almost 6%, and an EC down to 2.1 MJ/mol,²⁰ and (ii) by increasing the pressure up to 4 bar, which increases the rate coefficient for eq 3, and resulted in a NO_x yield up to 6% (being 94% NO_2 , hence beneficial for fertilizer applications), with an EC down to 1.8 MJ/mol and a NO_x production rate of 69 g/h.¹⁹ Despite these promising initial results for nitrogen fixation in order to be up-scaled at an industrial level, it will still be necessary not only to improve the values for the EC and NO_x yield but also to improve the electrical stability and the reproducibility of the technology. For this reason, studies on the electrical characterization have been performed on different gliding arc designs.^{21,22} Most of the time, the electrical stability in a GAP is successfully achieved through the utilization of external resistors.^{9,16,20,23–26} Nevertheless, the impact of these resistors on the NO_x yield and EC is poorly discussed in the literature. Indeed, most of the time, the reported values of the EC are calculated by considering the power directly injected in the plasma as an input value, without estimation of the loss of power into the resistors by the Joule effect. Therefore, in the present paper, a variable resistor has been implemented in a series of our DC power supply to stabilize the plasma, and the impact of the resistance has been systematically evaluated on both the NO_x yield and energy cost of the process. In the

second step and because of the obtained results, an alternative approach has been implemented to efficiently stabilize the discharge by using an inductor instead of an external resistor. Again, a complete characterization of the stabilization efficiency and also of the process performance in terms of NO_x yield and EC has been realized.

EXPERIMENTAL SETUP

Gliding Arc Reactor. Figure 1 shows a schematic view of the experimental setup. The reactor body is grounded and electrically

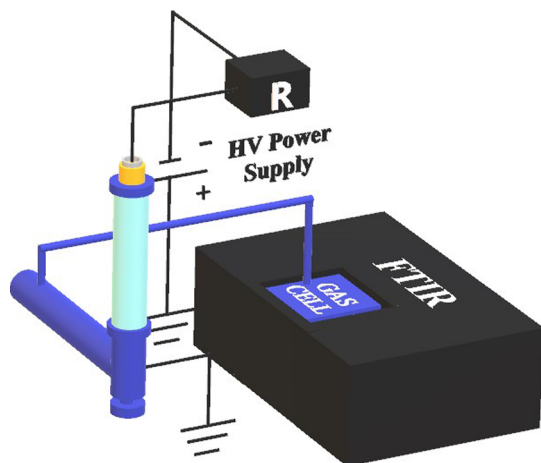


Figure 1. Scheme of the experimental setup highlighting the electrical circuit and FTIR position. The cathode is located inside the highlighted yellow cylinder. The gas cell is connected to the exhaust of the GAP.

connected to the anode. The cathode of the reactor is connected to a DC power supply (Technix SR12KV-15KW) through either a resistor R , which can be set to assume equivalent resistance values between 1 and 19 $\text{k}\Omega$ (configuration shown in Figure 2), or a 100 mH inductance L (Figure 2b).

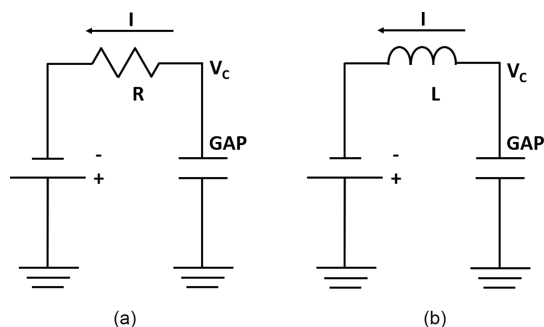


Figure 2. Electrical diagram of the setup with the configuration using a variable R (a) and L (b). V_c and I are highlighted.

The power supply has a negative polarity, providing an output voltage and current of up to 12 kV and 1.25 A, respectively. The cathode voltage V_c is measured with a high voltage probe (Picotech TA044 1000:1), and the arc current I is measured with a current probe (Tektronix TCP303) and a signal amplifier (Tektronix TCPA300). Both signals are recorded on a Tektronix TDS 2012B oscilloscope.

The details of the stainless steel electrodes in the gliding arc reactor are schematized in Figure 3. The inner diameters of the electrodes are 17.5 and 14.2 mm for the cathode and the anode, respectively. The cathode is insulated from the body of the reactor through a Teflon fit and is separated from the anode, which is directly screwed on the

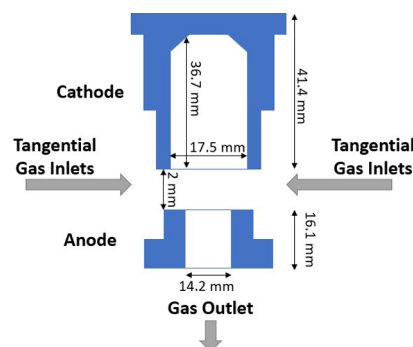


Figure 3. Scheme of the electrodes in which some of the most significant dimensions are reported.

reactor body, leaving 2 mm between the two electrodes. A high voltage is applied to the cathode until the dielectric breakdown of the gas between the two electrodes occurs. The current provided by the power supply is then increased to sustain a stable arc between the electrodes.

The gas is injected between the two electrodes through six tangential inlets, which are schematized in Figure 4, generating a

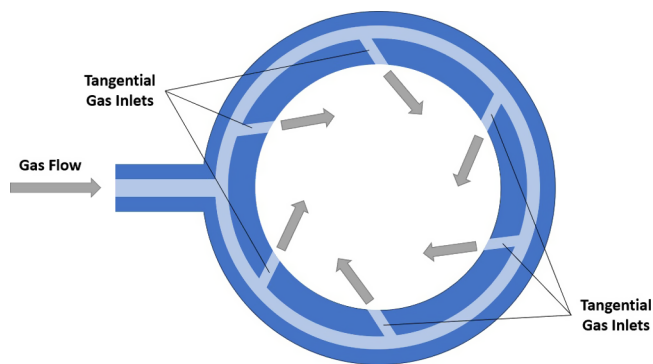


Figure 4. Scheme of the horizontal section indicating the six tangential inlets. The gas is directly injected between the electrodes.

vortex-like shape. Having a cathode wider than the anode forces the flow to operate in the reverse vortex flow (RVF) regime. This configuration ensures a better heat insulation on the cathode walls, the confinement of the arc in the center of the electrodes, and an improvement in the fraction of the gas flowing through the arc.^{17,18} The gas then flows into the body of the reactor, where the pressure is monitored with a manometer and, subsequently, is safely expelled through an exhaust. The GAP reactor operates at atmospheric pressure. A 20 cm diameter industrial fan pointed toward the reactor is used to cool the reactor walls down in a controlled way.

FTIR Absorption Analysis. The exhaust of the reactor is connected to an external gas cell, where the NO and NO_2 concentrations are measured with a Vertex 80v FTIR (Bruker) spectrometer. The internal deuterated lanthanum α -alanine-doped triglycine sulfate detector in the mid-IR region is used for absorbance measurement. The gas cell length is approximately 125 mm and is equipped with two ZnSe windows. A 2 mm aperture is used, which gives a resolution of 1 cm^{-1} . For each measurement, 20 spectra acquired in the range between 1000 and 3500 cm^{-1} were averaged. In order to obtain the absolute densities for the produced NO_x species, a calibration was performed using gas mixtures of 1% NO mixed in Ar and 2% NO_2 in Ar. The statistical error associated with the absorbance value is determined by repeating measurements for the same experimental conditions and estimated to be on the order of 1% of the measured values.

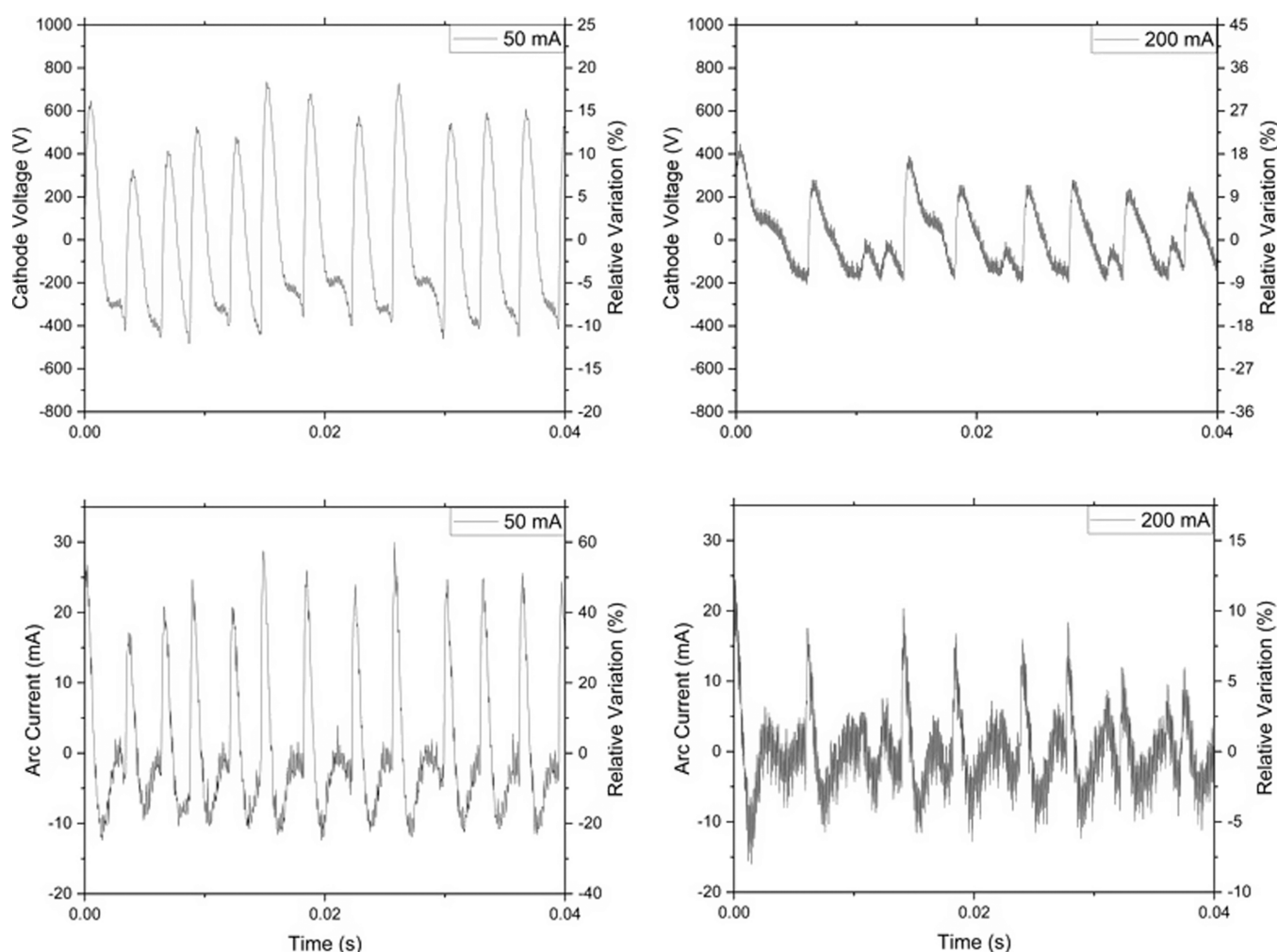


Figure 5. Temporal behavior of V_C (top) and I (bottom), where only the AC component is shown. R was set at 19 k Ω . The spectra were acquired with $\langle I \rangle$ equal to 50 mA (left) and 200 mA (right). The same curve also represents the relative variation, expressed as a percentage of the DC component of the signal ($\langle V_C \rangle$ and $\langle I \rangle$), with the corresponding numbers given at the right y-axis.

METHODOLOGY

The GAP presented in this work is always operated with a gas mixture of 5 slm (standard liters per minute) of N_2 and 5 slm of O_2 . The mean arc current $\langle I \rangle$ is evaluated as the statistical average of all the I measured with the oscilloscope during one acquisition and varies between 50 and 200 mA when the resistor is used (Figure 2) and between 275 and 500 mA when the inductor is employed (Figure 2). Indeed, in the latter case, it was not possible to ignite a plasma for $\langle I \rangle \leq 250$ mA. The mean cathode voltage $\langle V_C \rangle$ is also evaluated as the statistical average of all the V_C measured during an oscilloscope acquisition.

Electrical Characterization. Figure 5 shows, as an example, for $R = 19$ k Ω , the evolution of the time-resolved signal of V_C and I for two values of the mean arc current $\langle I \rangle$ in the GAP. The signal oscillation from $\langle I \rangle$ and the mean cathode voltage $\langle V_C \rangle$ ($\langle I \rangle$ and $\langle V_C \rangle$ correspond to the DC components of V_C and I) are shown both in terms of absolute and relative variations. V_C (corresponding to the voltage difference between the electrodes as the anode is grounded) describes the length of the arc as a function of time.²¹ At lower $\langle I \rangle$, the V_C and I signals show the typical "restrike" regime, characterized by intense spikes. These are caused by the arc, which rapidly elongates, until the voltage difference between

two points of the column is high enough to cause an electric breakdown, shortening the arc.^{21,27} With a constant input gas flow rate, the fluctuations of V_C decrease as $\langle I \rangle$ is increased, moving to a "steadier" state, where the arc elongations are milder. Indeed, an increase of $\langle I \rangle$ is reported to decrease the boundary layer of the arc,^{21,27} thus decreasing the drag effect applied by the gas flow. Despite the difference in the $\langle I \rangle$ range used for the measurements with R and L not allowing for a direct comparison, a milder effect is observed with L , as shown in Figure 6, where the relative variations of V_C and I are comparable for the two values of $\langle I \rangle$ and are, overall, stronger than what was observed with the resistance at $\langle I \rangle$ equal to 200 mA. The steep I and V_C variations typical of the "restrike" mode are not present, and the signal is dominated by Helmholtz resonance (typically reported to be of several kHz²¹), which is suppressed with the external resistor. The difference in the time scales should be noted.

It is important to mention that without a resistor or an inductor, it is not possible to sustain the plasma in the studied conditions because the discharge is too unstable. In this configuration, arcing occurs; however, due to the high current and voltage fluctuations, the arc extinguishes before it can be extended. This rapidly results in the electrodes being damaged. When such elements are added to the electrical circuit, the

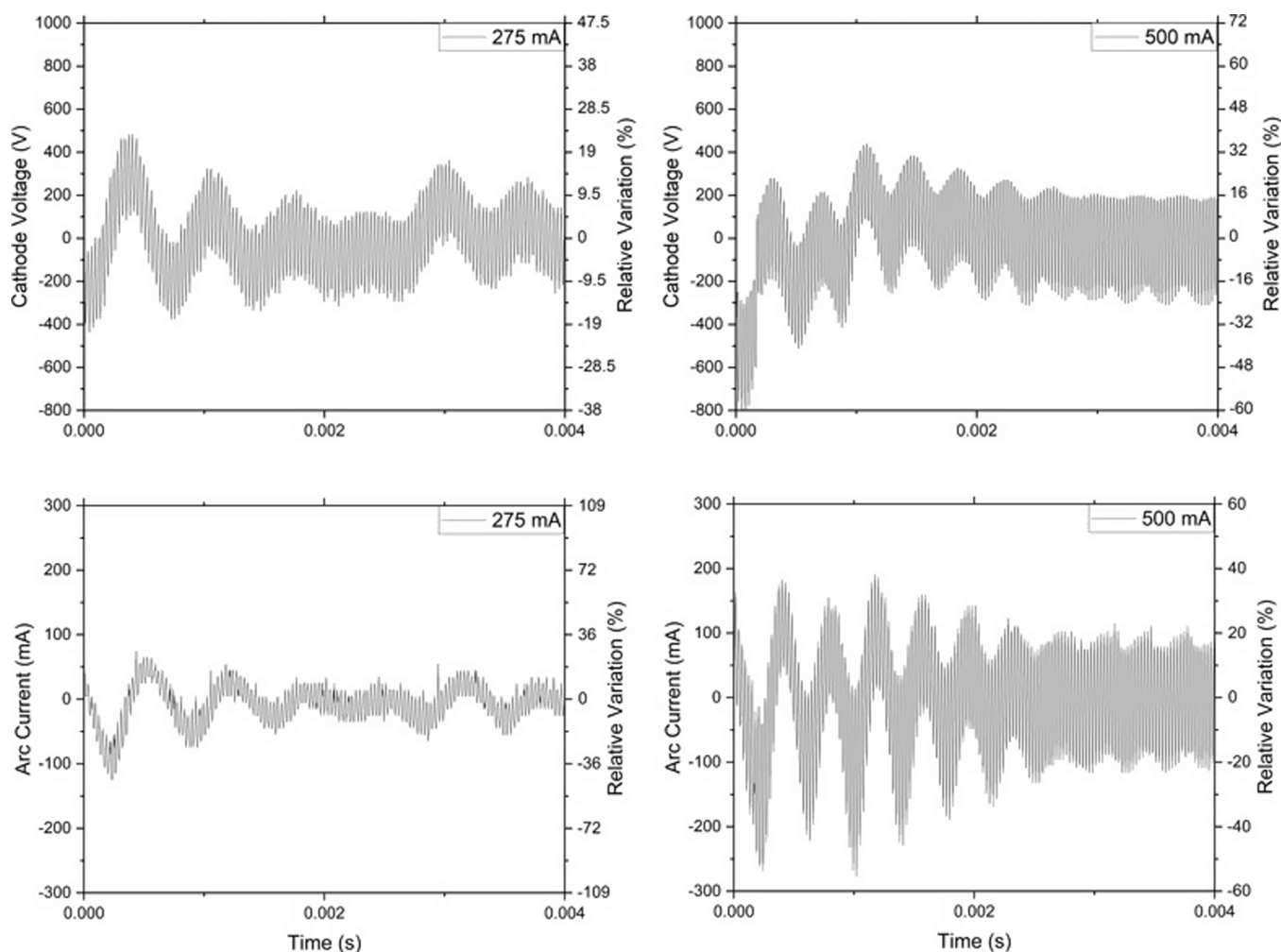


Figure 6. Temporal behavior of V_C (top) and I (bottom), where only the AC component is shown. L was set at 100 mH. The spectra were acquired with $\langle I \rangle$ of 275 mA (left) and 500 mA (right). The same curve also represents the relative variation, expressed as a percentage of the DC component of the signal ($\langle V_C \rangle$ and $\langle I \rangle$), with the corresponding numbers given at the right y-axis.

plasma can be sustained. As discussed in detail by Fridman et al.,²⁸ for an arc discharge to be stable, the differential resistance, defined as the derivative on $\langle I \rangle$ of the open circuit voltage ($\langle V_0 \rangle$) provided by the power supply of a resistive circuit (as is the case for the configuration in Figure 2), should be positive, as in the following equation²⁸:

$$\frac{d \langle V_0 \rangle}{d \langle I \rangle} = 2R - \frac{\langle V_0 \rangle}{\langle I \rangle} > 0 \quad (5)$$

which is true if:

$$\langle I \rangle > \frac{\langle V_0 \rangle}{2R} \quad (6)$$

as a consequence, a higher value of R allows the arc to be sustained at lower $\langle I \rangle$.

In order to strictly evaluate the instability level as a function of the studied conditions in this work, the standard deviations associated with the mean cathode voltage $\langle V_C \rangle$ and the mean arc current $\langle I \rangle$ values measured on the oscilloscope signals, normalized by $\langle V_C \rangle$ and $\langle I \rangle$, are considered representative of the instability level. Consequently, a larger relative variation can be associated with a higher instability level of the system. Using this definition, it can be observed in Figure 5 that the

instability level decreases as $\langle I \rangle$ increases and that, overall, the use of resistors seems to better stabilize the plasma.

The power provided to plasma P_p through the arc is evaluated as the integral over an arbitrary period of time t_0 of the product of V_C multiplied by the arc current I .

$$P_p = \frac{\int_0^{t_0} V_C(t) I(t) dt}{t_0} \quad (7)$$

This has to be distinguished from the total power P_T provided by the power supply, which takes into account the dissipation through the Joule effect on resistor R . With the assumption that the losses due to parasitic capacities and inductances are negligible, P_T can be evaluated by the following equation.

$$P_T = P_p + \langle I \rangle^2 R \quad (8)$$

At last, an important parameter for the characterization of the reactor performance is the energy cost EC, expressed in MJ/mol, representing the energy used per mole of fixated N_2 .

$$EC = \frac{P_T}{n_{NO_x} F} \quad (9)$$

where F is the input gas flow rate in the reactor and n_{NO_x} is the NO_x density.

Different versions of bidimensional gliding arc discharges exist and have been studied in the past, focusing on the thermal stability of the arc itself.²⁸ Notably, it is reported that the power dissipated by the arc per unit length plays an important role in defining the dynamics of the arc and its stability. Nevertheless, because of the specific geometry of the GAP, probing the region between the electrodes (where the arc develops) was not possible, making measurements of the arc length and radius or the local gas temperature not possible.

RESULTS AND DISCUSSION

Resistor. Figure 7 shows, on the top, the typical voltage–current characteristics for an arc discharge and, on the bottom,

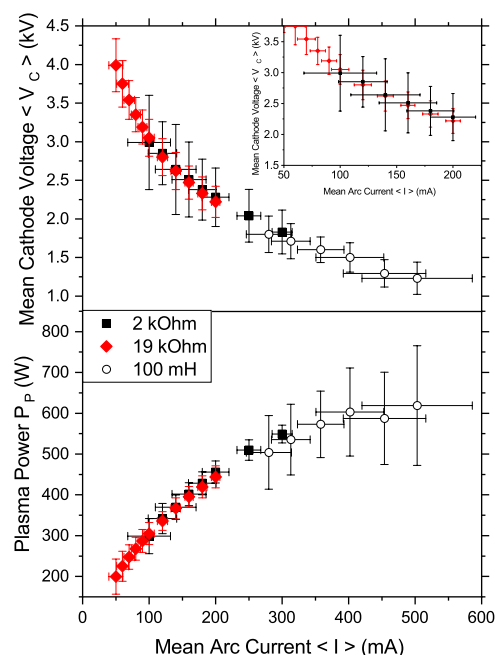


Figure 7. Mean cathode voltage (top) and the average P_P (bottom) as a function of the mean arc current $\langle I \rangle$ for two different values of R and for L .

the plasma power (P_P) as a function of $\langle I \rangle$ for two different values of R and L . According to the Steenbeck channel model for the column of an arc discharge, P_P/I presents a weak dependency on the arc current I , described by the following equation²⁹:

$$\frac{P_P}{I} = \frac{k_1}{(k_2 - \ln I)^2} \quad (10)$$

where k_1 and k_2 are constants, explaining both the trend observed for P_P in Figure 7 and, considering eq 7, for $\langle V_C \rangle$ in Figure 7. It is observed that $\langle V_C \rangle$ as a function of $\langle I \rangle$ is not affected by R and thus, only the results corresponding to the two extreme values used ($R = 2 \text{ k}\Omega$ and $R = 19 \text{ k}\Omega$) are shown. Likewise, the same behavior is observed for P_P . On average, it can be concluded that the arc elongation is not affected by any resistance in series with the reactor. The reported error bars correspond to the standard deviation measured for $\langle I \rangle$ and $\langle V_C \rangle$ based on the results shown in Figure 5 and are, as explained, associated with the instability of the discharge. From

the discussed results, it appears that for a given value of $\langle I \rangle$, the instability decreases when increasing R . This highlights the importance of the resistance in order to improve the stability of the discharge by limiting the $\langle I \rangle$ fluctuations. As previously discussed, a direct effect of increasing the arc stability through the value of R is that the plasma can be sustained using lower $\langle I \rangle$ and P_P when increasing R . In this work, for each value of R , the lowest applied values of $\langle I \rangle$ and P_P correspond to the minimum value that allowed the plasma to be sustained. The maximum $\langle I \rangle$ applied using R was instead limited by the power rating of the resistors. The R value could also be set to $1 \text{ k}\Omega$; however, with this configuration, the plasma failed to ignite presenting a similar behavior as described at the beginning of the section in the absence of any resistor or inductor. These data confirm previous reports revealing the efficiency of an external resistor in order to stabilize GAP discharges.

Concerning the effect of the resistor on the process in terms of yield and EC, the yield of NO_x (NO_2 and NO) as a function of P_P was measured for the two extreme values of R and is shown in Figure 8. The error in the NO_x yield is obtained by

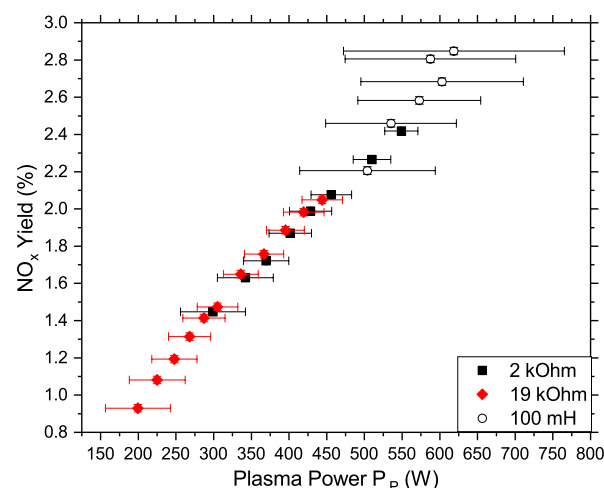


Figure 8. NO_x yield as a function of the P_P . The yield linearly increases with the plasma power.

propagating the error in the FTIR absorbance measurements. It is observed that the NO_x yield linearly increases with P_P , reaching a maximum of $2.08(2) \%$ ($R = 19 \text{ k}\Omega$) and $2.42(2) \%$ ($R = 2 \text{ k}\Omega$). The results are in line with the previous works reporting a linear dependency between the NO_x concentration and the specific energy input (i.e., P_P per liter of input gas).³⁰ The yield is therefore found to be independent of the choice of R . As previously discussed, the value of R affects I and V_C fluctuations of the arc rather than their mean value. Thus, the specific energy input is, on average, not affected by the R value, explaining the obtained trend.

Figure 9 reports the EC, evaluated according to eq 9, using as input power P_T (9) and P_P (9), respectively. Focusing on Figure 9, considering the error bars, it is shown that increasing P_P does not significantly impact the EC. In this case, the average value of the EC evaluated from P_P is estimated to be $2.82(6) \text{ MJ/mol}$, close to the best-reported results in literature.^{12,19,20} On the other hand, when P_T is used to calculate the EC (Figure 9a), a strong dependence of the EC as a function of P_P , which is strongly affected by R , is observed. Indeed the EC asymptotically increases with P_P , especially for

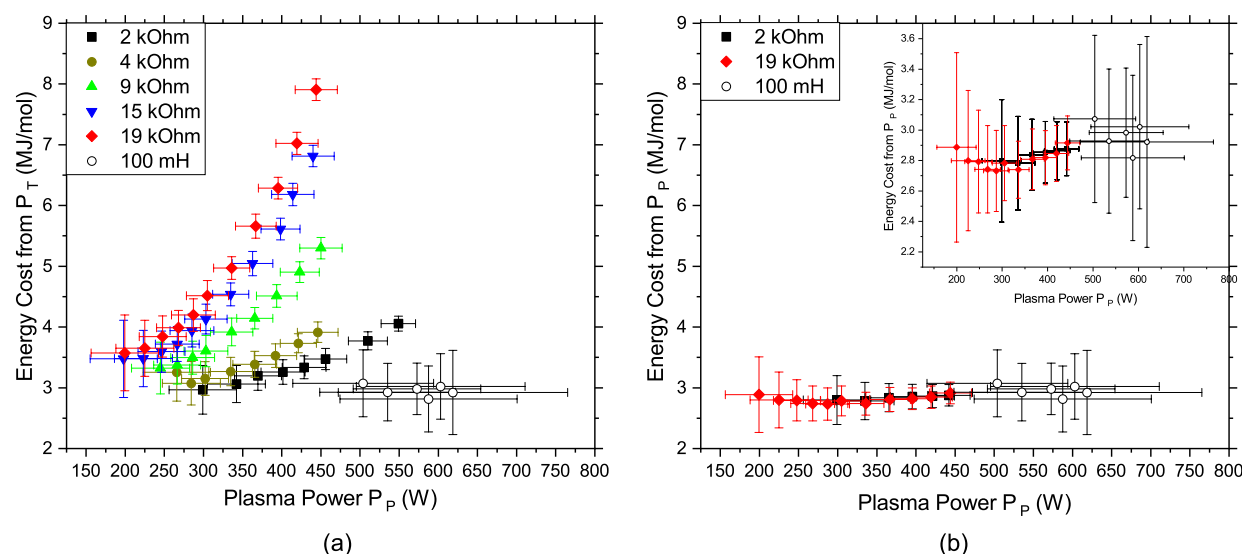


Figure 9. Evolution of EC as a function of P_p , when calculated based on (a) P_T , hence including the Joule dissipation by R , and (b) P_p , hence only due to the energy injected in the plasma. The latter is reported with two different scales and only two sets of points (i.e., $R = 2 \text{ k}\Omega$ and $R = 19 \text{ k}\Omega$) out of five are reported, to avoid excessive overlapping.

high values of R , for which, in the worst case, $EC = 7.9(2) \text{ MJ/mol}$. The difference in EC between the two situations obviously originates from the power dissipated on the resistor by the Joule effect. In order to better visualize this effect, Figure 10 shows the percentage of power effectively injected

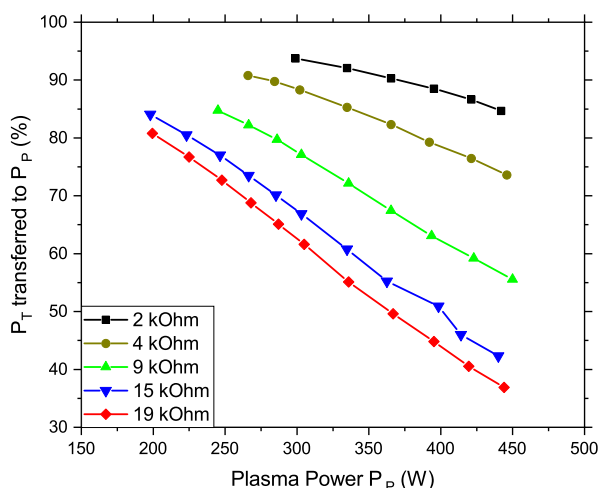


Figure 10. Fraction of P_T transferred to P_p , for different values of R , as a function of P_p . At higher R , a larger fraction of the power is lost through Joule heating.

into the plasma as a function of P_p for different values of R . It clearly appears that for the worst conditions ($R = 19 \text{ k}\Omega$ and $P_p = 450 \text{ W}$), only 35% of P_T is utilized by the plasma, while the rest is lost by the Joule effect. This clearly demonstrates that even if the utilization of an external resistor to stabilize the plasma is successful, the price to pay is sometimes a very strong decrease in the energy efficiency of the process when considering the applied power, which is indeed required for evaluating the industrial applicability.

Inductor. In order to avoid the loss in energy efficiency, this work suggests, as an alternative, the use of an inductor instead of external resistors. Therefore, it has been evaluated how this new approach allows for a stabilization of the plasma

and how it affects the process performance. In terms of plasma stabilization, the first observation is that it was not possible to ignite the plasma for $\langle I \rangle$ lower or equal to 250 mA because of the instabilities at low $\langle I \rangle$. On the other hand, it can be observed in Figures 7 and 8 that the results obtained when utilizing the inductor are consistent with the ones obtained in the conventional setup (utilizing R), but reveal bigger standard deviations on the $\langle I \rangle$ and $\langle V_C \rangle$ and therefore $\langle P_p \rangle$ values. In terms of relative instabilities, the measurements obtained with L show an average standard deviation of 12% for $\langle I \rangle$ and 13% for $\langle V_C \rangle$, which is comparable to what was observed for the measurements with R when the lower possible $\langle I \rangle$ was approached. It can therefore be concluded that the stabilization effect when utilizing the inductor approach is lower than that when utilizing the external resistor. Nevertheless, this does not prevent the ignition of the plasma for electrical conditions that are compatible with industrial applications (high current, high power, i.e., higher than with the resistors). Overall a positive effect was observed on both NO_x yield (Figure 8) and EC (Figure 9). Indeed, Figure 8 clearly shows a higher NO_x yield (up to 3%) when using an inductor, due to the higher P_p . Figure 9 illustrates that the EC based on P_p is only slightly higher (3 MJ/mol, again due to the higher P_p), but importantly, the EC based on P_T is also limited to this 3 MJ/mol, hence much lower than when using resistors, where the EC went up to 7.9 MJ/mol. This is very striking and shows that in combination with the clearly higher NO_x yield, using an inductor is really promising for industrial applications, where the EC based on the total power should be considered.

CONCLUSIONS

This work discussed the impact of passive electric components used to stabilize a GAP discharge on the stability level and the process performance (NO_x yield and EC). Resistors are the dominant choice in literature, as they enhance the stability of the arc discharge by limiting the fluctuations of the arc itself. However, the impact on the overall EC due to external resistors should not be neglected since, as reported, it can dramatically increase the total power consumption of the system. The GAP presented in this work achieved the lowest

energy cost, based on the energy provided to the plasma (P_p), of 2.82(6) MJ/mol, which is quite close to the most recent best results in the literature, i.e., 2.1–2.5 MJ/mol for an RGA,^{16,20} 2.0 MJ/mol for atmospheric pressure MW plasma,¹² and 1.8 MJ/mol for an enhanced pressure RGA.¹⁹ However, after considering the power lost due to Joule dissipation, this translates to an overall energy cost of up to 7.9 MJ/mol according to the choice of the resistance. It has been demonstrated that replacing the resistor with an inductor also allows for a decent stabilization of the discharge and, most importantly, avoids the loss of power through Joule dissipation. Both of the passive electric components tested in this work generally seem to play a negligible role in the chemistry of the plasma. Both with the resistor and with the inductor, the NO_x yield showed a linear dependence with P_p , with a best-measured value of 2.85(2) % corresponding to the highest P_p . By further increase, higher NO_x yields could be achieved with little repercussions on the EC due to P_p alone if the highlighted trend is valid for higher P_p . Furthermore, when using an inductor, also the EC based on total (applied) power remains constant upon increasing power, being as low as 3 MJ/mol. This is in contrast to the case when using external resistors, where the EC based on total power rises with power. To conclude, this work strongly suggests that an inductor should be preferred for discharge stabilization in order to achieve a competitive overall EC (i.e., based on applied power) for plasma nitrogen fixation with a GAP.

■ ASSOCIATED CONTENT

SI Supporting Information

The Supporting Information is available free of charge at <https://pubs.acs.org/doi/10.1021/acssuschemeng.3c08257>.

Additional details on the method for the FTIR data analysis (PDF)

■ AUTHOR INFORMATION

Corresponding Author

Filippo Manaigo – Research Group ChIPS, Department of Chemistry, University of Mons, 7000 Mons, Belgium;
Research Group PLASMANT, Department of Chemistry, University of Antwerp, 2610 Antwerp, Belgium;
✉ orcid.org/0009-0008-2484-3578;
Email: filippo.manaigo@umons.ac.be

Authors

Omid Samadi Bahnamiri – Research Group ChIPS, Department of Chemistry, University of Mons, 7000 Mons, Belgium
Abhyuday Chatterjee – Research Group ChIPS, Department of Chemistry, University of Mons, 7000 Mons, Belgium
Adriano Panepinto – Materia Nova Research Center, Parc Initialis, 7000 Mons, Belgium
Arnaud Krumpmann – Materia Nova Research Center, Parc Initialis, 7000 Mons, Belgium
Matthieu Michiels – Materia Nova Research Center, Parc Initialis, 7000 Mons, Belgium
Annemie Bogaerts – Research Group PLASMANT, Department of Chemistry, University of Antwerp, 2610 Antwerp, Belgium; ✉ orcid.org/0000-0001-9875-6460
Rony Snyders – Research Group ChIPS, Department of Chemistry, University of Mons, 7000 Mons, Belgium;

Materia Nova Research Center, Parc Initialis, 7000 Mons, Belgium

Complete contact information is available at:

<https://pubs.acs.org/doi/10.1021/acssuschemeng.3c08257>

Notes

The authors declare no competing financial interest.

■ ACKNOWLEDGMENTS

The research is supported by the FNRS-FWO project “NITROPLASM”, EOS O005118F.

■ REFERENCES

- (1) Frink, C.; Waggoner, P.; Ausubel, J. Nitrogen fertilizer: Retrospect and prospect. *Proc. Natl. Acad. Sci. U.S.A.* **1999**, *96*, 1175–1180.
- (2) Frost, D. C.; McDowell, C. A.; Bawn, C. E. H. The dissociation energy of the nitrogen molecule. *Proc. R. Soc. Lond. A* **1956**, *236*, 278–284.
- (3) Graham, P.; Vance, C. Nitrogen fixation in perspective: an overview of research and extension needs. *Field Crops Res.* **2000**, *65*, 93–106.
- (4) Cherkasov, N.; Ibhaden, A.; Fitzpatrick, P. A review of the existing and alternative methods for greener nitrogen fixation. *Chem. Eng. Process* **2015**, *90*, 24–33.
- (5) Clomburg, J. M.; Crumbley, A. M.; Gonzalez, R. Industrial biomanufacturing: The future of chemical production. *Science* **2017**, *355*, No. aag0804.
- (6) Rafiqul, I.; Weber, C.; Lehmann, B.; Voss, A. Energy efficiency improvements in ammonia production-perspectives and uncertainties. *Energy* **2005**, *30*, 2487–2504.
- (7) IEA *Global CO2 emissions in 2019*; 2020.
- (8) Patil, B.; Wang, Q.; Hessel, V.; Lang, J. Plasma N₂-fixation: 1900–2014. *Catal.* **2015**, *256*, 49–66 Plasmas for enhanced catalytic processes (ISPCEM 2014)..
- (9) Vervloessem, E.; Aghaei, M.; Jardali, F.; Hafezkhani, N.; Bogaerts, A. Plasma-Based N₂ Fixation into NO_x: Insights from Modeling toward Optimum Yields and Energy Costs in a Gliding Arc Plasmatron. *ACS Sustain. Chem. Eng.* **2020**, *8*, 9711–9720.
- (10) Sarafraz, M. M.; Tran, N. N.; Nguyen, H.; Fulcheri, L.; Burton, R.; Wadewitz, P.; Butler, G.; Kirton, L.; Hessel, V. Tri-fold process integration leveraging high- and low-temperature plasmas: From biomass to fertilizers with local energy and for local use. *J. Adv. Manuf. Process.* **2021**, *3*, No. e10081.
- (11) Bahnamiri, O. S.; Verheyen, C.; Snyders, R.; Bogaerts, A.; Britun, N. Nitrogen fixation in pulsed microwave discharge studied by infrared absorption combined with modelling. *Plasma Sources Sci. Technol.* **2021**, *30*, No. 065007.
- (12) Kelly, S.; Bogaerts, A. Nitrogen fixation in an electrode-free microwave plasma. *Joule* **2021**, *5*, 3006–3030.
- (13) Vervloessem, E.; Gorbanev, Y.; Nikiforov, A.; De Geyter, N.; Bogaerts, A. Sustainable NO_x production from air in pulsed plasma: elucidating the chemistry behind the low energy consumption. *Green Chem.* **2022**, *24*, 916–929.
- (14) Pei, X.; Gidon, D.; Graves, D. Specific energy cost for nitrogen fixation as NO_x using DC glow discharge in air. *J. Phys. D: Appl. Phys.* **2020**, *53*, No. 044002.
- (15) Bogaerts, A.; Neyts, E. C. Plasma Technology: An Emerging Technology for Energy Storage. *ACS Energy Letters* **2018**, *3*, 1013–1027.
- (16) Jardali, F.; Van Alphen, S.; Creel, J.; Ahmadi Eshtehardi, H.; Axelsson, M.; Ingels, R.; Snyders, R.; Bogaerts, A. NO_x production in a rotating gliding arc plasma: potential avenue for sustainable nitrogen fixation. *Green Chem.* **2021**, *23*, 1748–1757.
- (17) Ramakers, M.; Medrano, J. A.; Trenchev, G.; Gallucci, F.; Bogaerts, A. Revealing the arc dynamics in a gliding arc plasmatron: a

better insight to improve CO₂ conversion. *Plasma Sources Science and Technology* **2017**, *26*, 125002.

(18) Trenchev, G.; Kolev, S.; Bogaerts, A. A 3D model of a reverse vortex flow gliding arc reactor. *Plasma Sources Science and Technology* **2016**, *25*, No. 035014.

(19) Tsonev, I.; O'Modhrain, C.; Bogaerts, A.; Gorbanev, Y. Nitrogen Fixation by an Arc Plasma at Elevated Pressure to Increase the Energy Efficiency and Production Rate of NO_x. *ACS Sustainable Chem. Eng.* **2023**, *5*, 1888–1897.

(20) Van Alphen, S.; Ahmadi Eshtehardi, H.; O'Modhrain, C.; Bogaerts, J.; Van Poyer, H.; Creel, J.; Delplancke, M.-P.; Snyders, R.; Bogaerts, A. Effusion nozzle for energy-efficient NO_x production in a rotating gliding arc plasma reactor. *Chem. Eng. J.* **2022**, *443*, No. 136529.

(21) Wu, C.; Pan, W. Unsteadiness in non-transferred dc arc plasma generators. *Theor. Appl. Mech. Lett.* **2011**, *1*, No. 024001.

(22) Kusano, Y.; Salewski, M.; Leipold, F.; Zhu, J.; Ehn, A.; Li, Z.; Alden, M. Stability of alternating current gliding arcs. *Eur. Phys. J. D* **2014**, *68*, 319.

(23) Ramakers, M.; Trenchev, G.; Heijkers, S.; Wang, W.; Bogaerts, A. Gliding Arc Plasmatron: Providing an Alternative Method for Carbon Dioxide Conversion. *ChemSusChem* **2017**, *10*, 2642–2652.

(24) Zhang, H.; Li, L.; Li, X.; Wang, W.; Yan, J.; Tu, X. Warm plasma activation of CO₂ in a rotating gliding arc discharge reactor. *J. of CO₂ Util.* **2018**, *27*, 472–479.

(25) Zhang, H.; Du, C.; Wu, A.; Bo, Z.; Yan, J.; Li, X. Rotating gliding arc assisted methane decomposition in nitrogen for hydrogen production. *Int. J. Hydrog. Energy* **2014**, *39*, 12620–12635.

(26) Trenchev, G.; Kolev, S.; Wang, W.; Ramakers, M.; Bogaerts, A. CO₂ Conversion in a Gliding Arc Plasmatron: Multidimensional Modeling for Improved Efficiency. *J. Phys. Chem. C* **2017**, *121*, 24470–24479.

(27) Rat, V.; Mavie, F.; Coudert, J. F. Electric Arc Fluctuations in DC Plasma Spray Torch. *Plasma Chem. Plasma Process.* **2017**, *37*, 549–580.

(28) Fridman, A.; Nester, S.; Kennedy, L. A.; Saveliev, A.; Mutaft-Yardimci, O. Gliding arc gas discharge. *Prog. Energy Combust. Sci.* **1999**, *25*, 211–231.

(29) Fridman, A.; Kennedy, L. A. *Plasma physics and engineering*, 2nd ed.; CRC Press, 2011.

(30) Chen, H.; Wu, A.; Mathieu, S.; Gao, P.; Li, X.; Xu, B. Z.; Yan, J.; Tu, X. Highly efficient nitrogen fixation enabled by an atmospheric pressure rotating gliding arc. *Plasma Processes Polym.* **2021**, *18*, No. 2000200.